J Solid State Electrochem (2003) 7: 208 – 216
DOI 10.1007/s10008-002-0299-y

ORIGINAL PAPER

Eduardo Méndez · Ana M. Castro Luna
María F. Cerdá · Alvaro W. Mombrú
Carlos F. Zinola · María E. Martins

Topography changes of rhodium electrodes induced by the application of fast periodic potential routines

Received: 20 November 2001 / Accepted: 11 June 2002 / Published online: 14 August 2002

Abstract The surface structure of polycrystalline rhodium electrodes in contact with aqueous sulfuric acid was modified by chemical etching with hot concentrated acid or by applying fast square waves with an upper potential equal to 1.55 V and a lower potential within the –0.75 V to –0.35 V range. Polycrystalline rhodium and chemical etched electrodes were characterized by voltammetry, Cu underpotential deposition (upd) and X-ray diffraction. For electrofaceted surfaces were used voltammetry, Cu upd and SEM, revealing that two modified rhodium electrodes exhibit similar voltammetric characteristics as those found for Rh(111) and Rh(110) single crystals, and a third surface with an equal distribution of (110) and (111) planes. In addition, the upd of Cu on those surfaces corroborated the existence of those crystallographic planes. SEM micrographs show surface structures with a high density of terraces and steps. A mechanism of faceting is proposed.

Keywords Rhodium · Electrochemical faceting · Chemical etching

Introduction

The electrochemical faceting of noble metals is a well-established procedure for the development of modified surfaces [1, 2, 3, 4, 5]. Nevertheless, not only massive bulk metals can be modified by this procedure since also crystallites of noble metals have been deposited on a carbon substrate, resulting in a surface with a preferred crystallographic orientation, as deduced from SEM, STM and X-ray diffraction studies [6].

Most of the work related to electrofaceting of noble metals has been performed on platinum [7, 8, 9, 10, 11, 12, 13] and gold [14, 15], and a mechanism for their formation has been furnished. Several processes of electrodissolution and electrocrystallization are often involved in electrofaceting, which occur with a progressive transformation that leads to the formation of stepped surfaces showing a preferred crystallographic orientation [10, 16, 17]. The electrofaceted electrodes have been characterized by cyclic voltammetry [7, 13, 16, 17], metal underpotential deposition (upd) [4, 9], scanning electron microscopy (SEM) [18] and scanning tunneling microscopy (STM) [4, 19]. The application of fast periodic potential routines to platinum electrodes results in two stable electrofaceted surfaces which have been named as Pt(100)-like and Pt(111)-like surfaces, taking into account that the voltammograms run in aqueous sulfuric acid resemble those of Pt(100) and Pt(111) single crystals subjected to several hundred potential cycles within the potential domain of the thermodynamic stability of water [20]. Thus, these surfaces exhibit an extensive change in morphology induced by oxygen adsorption, revealing the formation of a highly disordered topography, which in turn also displays a preferred crystallographic orientation. The comparison with the voltammetric behaviour of different platinum single crystals within the 0.05–1.45 V potential range allowed us to recognize that Pt(100)-like and Pt(111)-like surfaces resemble those of Pt(310) and Pt(320), respectively [21]. Moreover, Pt(310) and Pt(320) surfaces are obtained also when repetitive potential scans are applied to other single crystals, suggesting that these surfaces exhibit crystallographic planes with an energetically favourable configuration [22, 23].

A.M. Castro Luna · M.E. Martins (✉)
Instituto de Investigaciones Fisicoquímicas Teóricas
y Aplicadas (INIFTA), Universidad Nacional de la Plata,
La Plata, Buenos Aires, Argentina
E-mail: mmartins@inifta.unlp.edu.ar
Fax: + 54-221-4254642

E. Méndez · M.F. Cerdá · C.F. Zinola
Laboratorio de Electroquímica Fundamental y Bioelectroquímica,
Facultad de Ciencias, Universidad de la República,
Iguá 4225, 11400 Montevideo, Uruguay

A.W. Mombrú
Laboratorio de Cristalografía y Química del Estado Sólido,
DEQUIFIM, Facultad de Química, Universidad de la República,
Gral. Flores 2124, CC 1157, Montevideo, Uruguay

In contrast to platinum and gold, the literature dealing with the electrofaceting of rhodium surfaces is scarce. Thus, the articles involve mainly the application of fast periodic triangular potential perturbations in aqueous acid media within the range of thermodynamic stability of water, leading to the development of highly stepped surfaces with preferred crystallographic orientations [24, 25].

The aim of this work is to obtain rhodium faceted surfaces either through chemical etching or by electrochemical methods, applying new routines developed in the laboratory which involve fast periodic square wave potential perturbations where both the cathodic and the anodic switching potentials are located out of the potential range of the thermodynamic stability of water. These surfaces were further characterized.

Experimental

The experiments were performed in a three-body electrochemical cell, consisting of a 30 mL main chamber joined through a Luggin-Haber capillary to a reservoir for the reference electrode, and through a fritted porous plaque to another reservoir for the counter electrode.

Rhodium wires (0.1 and 0.05 mm in diameter, Goodfellow, 99.98%) soldered into soft glass tubes were used as working electrodes, cleaned in hot concentrated H_2SO_4 and rinsed thoroughly with Millipore-MilliQ water. These electrodes were subjected to a potentiodynamic cycling from 0.05 V to 1.20 V in aqueous 1 M H_2SO_4 (supporting electrolyte) at $v = 0.05$ V s^{-1}, until stabilized voltammograms were obtained. The real surface area of the working electrodes (0.017 cm^2 and 0.18 cm^2) was measured according to the usual procedures [26]. The counter electrode was a rhodium sheet (1 cm^2 geometric area, Goodfellow, 99.98%), and the reference electrode was a reversible hydrogen electrode (RHE). The potentials in the text are referred to the RHE scale. The electrolytic solutions were freed from dissolved oxygen by bubbling pure nitrogen (AGA, 99.998%) for 30 min before each experiment and over the solution during the experiment.

Potential routines used for the development of electrofaceted surfaces involved square waves with a lower switching potential in the $-0.75\ V \le E_l \le -0.35$ V range and an upper switching potential $E_u = 1.55$ V, applied at a frequency 5 kHz $\le f \le$ 35 kHz for a time t.

Cu upd experiments were performed in aqueous 10^{-4} M $CuSO_4$ in the supporting electrolyte at $v = 0.02$ V s^{-1}.

X-ray diffraction measurements were carried out using a Seifert-Scintag PADII diffractometer. The scans were performed with CuKα radiation ($\lambda = 1.5418$ Å), from $2\theta = 380$ to 720 in steps of 0.040, 3 s/step.

SEM micrographs were obtained with a JEOL scanning electron microscope, model JSM-5900 LV.

Results

Voltammetric behaviour of pc-Rh

The voltammetic behaviour of polycrystalline rhodium (pc-Rh) in aqueous 1 M H_2SO_4 is shown in Fig. 1a. The hydrogen-electrosorption potential domain extends from 0.05 V to 0.30 V, where an anodic current peak at 0.10 V with a shoulder at 0.12 V is observed. The cathodic potential region exhibits a current peak at 0.08 V

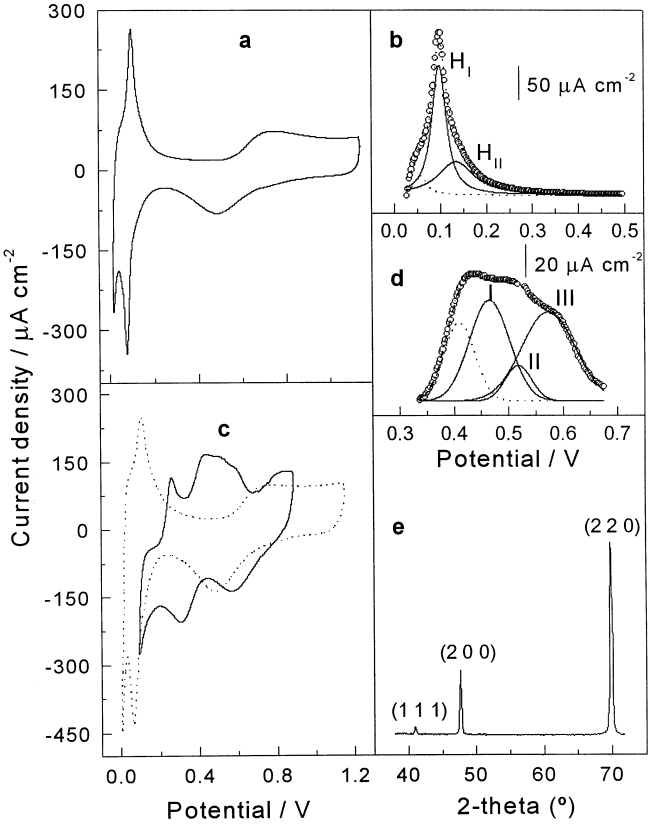

Fig. 1 **a** Cyclic voltammogram of pc-Rh in aqueous 1 M H_2SO_4; $v = 0.1$ V s^{-1}, $A = 0.017$ cm^2. **b** Graphical deconvolution of H-electrodesorption region: *open circles*, experimental data; *solid line*, lorentzian contributions corresponding to H adsorption states H_I and H_{II}; *dashed line*, contribution due to molecular hydrogen oxidation; $v = 0.1$ V s^{-1}, $A = 0.017$ cm^2. **c** Cyclic voltammogram of pc-Rh in aqueous 10^{-4} M $CuSO_4 + 1$ M H_2SO_4: *dashed line*, blank in aqueous 1 M H_2SO_4; $v = 0.02$ V s^{-1}, $A = 0.18$ cm^2. **d** Graphical deconvolution of Cu upd electrodesorption: *open circles*, experimental data; *solid line*, gaussian contributions corresponding to Cu upd dissolution from different crystalline sites; *dashed line*, Cu bulk electrodissolution; $v = 0.02$ V s^{-1}, $A = 0.18$ cm^2. **e** X-ray diffraction pattern of pc-Rh; $A = 1$ cm^2

with a shoulder at 0.11 V, whereas the hydrogen evolution reaction begins at $E = 0.04$ V. After graphical deconvolution of the H-electrodesorption potential region, two anodic current peaks located at 0.098 V and 0.134 V can be seen (Fig. 1b). On the other hand, the oxygen-electroadsorption region starts at 0.52 V and extends up to the anodic switching potential $E_{sa} = 1.2$ V, where a wide current contribution with a maximum located at 0.73 V is observed. Reversing the potential scan, oxygen electrodesorption is accomplished, partially overlapping the H-electroadsorption region. The potential of the O-electrodesorption current peak shifts towards negative values for $E_{sa} > 1.2$ V [27, 28, 29]. The voltammograms of pc-Rh in aqueous 10^{-4} M $CuSO_4 + 1$ M H_2SO_4, run from $E_{sa} = 0.9$ V down to $E_{sc} = 0.15$ V (Fig. 1c), exhibit in the negative-going potential scan several current contributions, namely, a current peak at ca. 0.6 V due to O-electrodesorption and

another one at 0.3 V corresponding to upd of Cu, whereas at $E = 0.2$ V bulk Cu electrodeposition takes place. In the positive-going potential scan a current peak located at 0.26 V corresponding to electrodissolution of bulk Cu is noticeable, whereas current contributions observed from 0.45 V to 0.70 V involve the electrodesorption of Cu upd from different crystallographic planes [16, 25]. The potential region of Cu upd was graphically deconvoluted (Fig. 1d), resulting for $E = 0.45$ V in three current contributions, namely peak I at 0.48 V, peak II at 0.53 V and peak III at 0.58 V. Current peak II corresponds to the (110) plane, while current peaks I and III to the (100) plane [30]. Current peak III has been also associated with the (111) plane [30]. Consequently, taking into account that from Cu upd results only (110) and (100) planes can be unequivocally assigned, X-ray diffraction analysis of pc-Rh was performed to resolve the uncertainty about the existence of the (111) planes (Fig. 1e). The results corroborate the absence of (111) planes and therefore allowed us to ascribe current peak III to the (100) planes.

Chemically etched Rh surface

When a pc-Rh electrode is immersed in boiling concentrated H_2SO_4 for 3 min and subsequently quenched in oxygen-free ultrapure water at room temperature, a voltammetric response different from the original one is obtained (Fig. 2a, dashed line). Thus, within the H-electrosorption potential domain an anodic current peak at 0.11 V and a cathodic current peak at 0.06 V are observed. The voltammogram corresponding to Cu upd on this modified Rh surface (Fig. 2a, solid line) reveals the presence of peak III at 0.58 V as the main contribution, indicating the prevalence of (111) planes [30]. Furthermore, a comparison of voltammograms of the Rh-modified surface with that of pc-Rh reveals that the H-electrosorption current peaks show an enhanced asymmetry with a potential peak difference $\Delta E_p = 0.05$ V, denoting a higher irreversibility. Consequently, H-electrosorption was studied at different sweep rates (v) (Fig. 2b, c), concluding that for the H-electrodesorption process the current peak increases linearly with ln v whereas the peak potential is independent of v, denoting a reversible behaviour of the adsorbed species. On the other hand, the H-electroadsorption process exhibits also a linear increase of the current peak with v, but the potential peak changes linearly with ln$v$, suggesting an irreversible process. The irreversibility observed for this electrofaceted surface is in agreement with that reported for Rh(111) single crystals in aqueous 10^{-4} M $H_2SO_4 + 0.1$ M $HClO_4$ [31, 32].

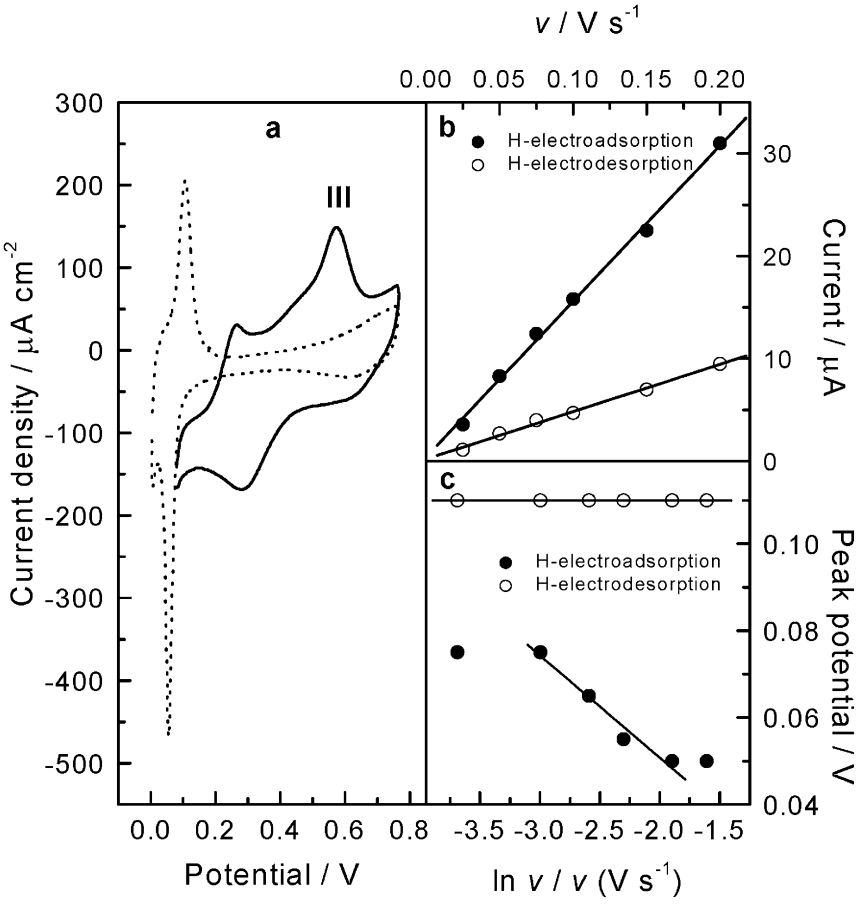

Fig. 2 **a** Cyclic voltammogram of chemically etched Rh in 10^{-4} M $CuSO_4 + 1$ M H_2SO_4: *dashed line*, blank in aqueous 1 M H_2SO_4; $v = 0.02$ V s^{-1}, $A = 0.18$ cm^2. **b** Current versus v plot for (*solid circles*) H-electroadsorption peak and (*open circles*) H-electrodesorption peak. **c** Peak potential versus ln v plot for (*solid circles*) H-electroadsorption peak and (*open circles*) H-electrodesorption peak

Electrofaceted surfaces

General features

Potential routines employed to achieve electrofaceted surfaces involved repetitive square wave signals, characterized by $E_u = 1.55$ V, -0.75 V $\leq E_l \leq -0.35$ V and a frequency 5 kHz $\leq f \leq$ 35 kHz. The parameters of the potential routines are gathered in Table 1, where the potential difference, $W = E_u - E_l$, was also taken into account. Voltammograms run after applying routines I to III show that three electrofaceted surfaces, Rh-I, Rh-II and Rh-III, are obtained (Fig. 3). The main features of the electrofaceted surfaces are related to the increase in height of the H-electrodesorption current peaks together with their sharpening as compared to those of pc-Rh (Fig. 3b). On the other hand, a greater cathodic charge density related to O-containing species for the three surfaces as compared with the original one is calculated. For Rh-I and Rh-III, new cathodic current contributions located at 0.73 V and 0.80 V are observed. It should be emphasized that after a continuous potential cycling within the 0.05–1.1 V range, the Rh-I and Rh-II electrodes are unchanged. However, Rh-III showed a progressive restructuring, reproducing finally a voltammetric profile resembling that of pc-Rh. Furthermore, the development of electrofaceting was followed through F, the ratio between the height of the H-electrodesorption current peak of the electrofaceted surface and the original one [16]. It has been found that a plot of F as a function of the applied frequency showed a maximum at 35 kHz (Fig. 4).

H-electrosorption region

The main differences in the H-electrosorption voltammetric profiles after the electrofaceting process are related to peak potentials, which in turn are helpful for the identification of the crystallographic planes of the surface. These values, together with those corresponding to pc-Rh and to chemically etched Rh surfaces, are assembled in Table 2. Furthermore, it should be pointed out that the degree of reversibility for the H-electrosorption reaction increases in the order Rh-I > pc-Rh > Rh-II [16]. Both the peak potential values and the degree of reversibility are in accordance with those already reported for Rh single crystals. Thus, the voltammetric behaviour of Rh-I and Rh-II electrodes resembles those of Rh(111) and Rh(110), respectively [30, 31, 32, 33, 34, 35]. The application of potential routine III leads to complex voltammetric behaviour in the H-electrosorption potential region as two superimposed but still distinguishable current peaks are observed, as is shown in the graphical deconvolution depicted in Fig. 5. Two redox couples are defined, i.e. the first at 0.104 V/0.078 V and the second at 0.097 V/0.087 V, which can be related to those redox couples observed for Rh-I and Rh-II, respectively (Table 2). Consequently, Rh-III can be described as a surface exhibiting an equivalent distribution of (110) and (111) crystallographic planes.

Table 1 Parameters of the square wave potential routines applied to the pc-Rh|aqueous 1 M H_2SO_4 interface for the development of Rh electrofaceted surfaces. E_l, lower potential limit; E_u, upper potential limit; $W = E_u - E_l$; f, frequency

Routine applied	Rh electrofaceted surface	E_l (V)	E_u (V)	W (V)	f (kHz)
I	Rh-I[a]	–0.35	1.55	1.90	35
II	Rh-II[b]	–0.55	1.55	2.10	35
III	Rh-III[b]	–0.75	1.55	2.30	5

O-electrosorption region

The O-electrosorption on electrofaceted Rh was voltammetrically investigated by applying a gradual increase of E_{sa} from 0.8 V to 1.3 V (Fig. 6a). It can be seen that O-electroadsorption extends from 0.55 V to 1.3 V, showing a broad current peak at ca. 0.75 V, whereas on reversing the potential scan a main cathodic current peak located at 0.43 V (Ic) and two new cathodic current peaks at 0.73 V (IIc) and 0.80 V (IIIc) are observed. These two cathodic peaks can be attributed to electrochemical processes taking place on the electrofaceted surface in the positive-going potential scan for $E_{sa} = 1.0$ V and $E_{sa} = 1.3$ V, respectively. It should be noticed that current peaks IIc and IIIc reported here have been observed only with Rh-I and Rh-III electrodes, both surfaces exhibiting (111) planes. In fact, on pc-Rh and Rh-II for which (111) planes are absent, no additional cathodic current peaks were observed after the application of the potential routines, concluding that

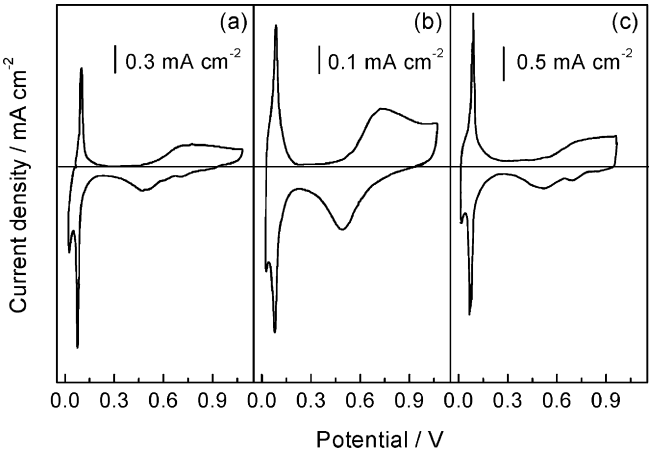

Fig. 3a–c Cyclic voltammograms of electrofaceted Rh surfaces in aqueous 1 M H_2SO_4 obtained by the application of fast periodic potential routines; $v = 0.1$ V s^{-1}. **a** Rh-I after application of routine I; $A = 0.017$ cm^2. **b** Rh-II after application of routine II; $A = 0.017$ cm^2. **c** Rh-III after application of routine III; $A = 0.18$ cm^2

oxygen species associated with current peaks located at 0.73 V and 0.80 V are preferentially formed on (111) planes. In order to obtain a deeper comprehension of O-electroadsorption/electrodesorption processes, the O region was graphically deconvoluted by means of gaussian contributions. Consequently, three anodic and three cathodic curves (Ia, IIa, IIIa and Ic, IIc, IIIc) reproduce the voltammogram obtained for $E_{sa} = 1.3$ V (Fig. 6b, solid lines). The current peaks of those curves are located at 0.77, 0.92 and 1.24 V within the anodic potential domain and at 0.43, 0.73 and 0.80 V in the cathodic one. A first inspection of the deconvoluted curves allows us to infer that curve Ic corresponds to the main O-electroreduction peak, whereas curves IIc and IIIc are related to the oxidation processes responsible for peaks IIa and IIIa. The charge densities involved within the three deconvoluted curves were calculated in terms of monolayers (ML) of adsorbed OH on Rh. Current contributions related to curves Ia and IIa involve a total anodic charge density equivalent to 2.45 ML, a figure that accounts for the contribution of curve Ia equivalent to 0.85 ML, and curve IIa to 1.60 ML. Curve IIIa involves an anodic charge equivalent to 1.26 ML up to $E_{sa} = 1.3$ V, but considering the complete gaussian curve, a value of 1.7 ML is calculated. Reversing the potential scan, curves IIIc, IIc and Ic involve a charge density equivalent to 0.34, 0.27 and 2.09 ML, respectively. Thus, from the experimental data it can be concluded that Ia + IIa = Ic + IIc.

SEM characterization of electrofaceted Rh surface

The surface topography of Rh-I and Rh-II were examined by SEM (Fig. 7). The application of routine I to pc-Rh (Fig. 7a) yields a surface with a high density of steps, terraces and kinks, revealing that the new topography contains high-index Miller planes (Fig. 7b). Thus, the micrographs show the formation of faceted grains of different sizes with well-defined borders forming angles in the 30–120° range. Besides, smaller faceted grains and a relatively large number of grains approaching faces with triangular shapes can be observed. The same features concerning the degree of surface faceting was observed also for Rh-II electrodes, showing topography with wide terraces and square-like steps (Fig. 7c). These surface topographies are similar to those reported for other electrofaceted metal surfaces [18].

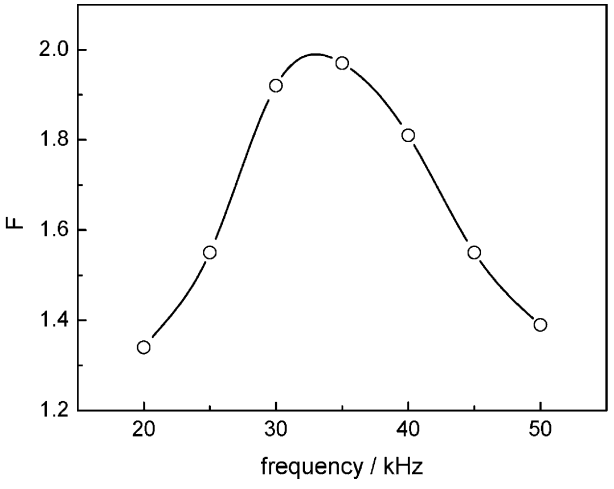

Fig. 4 Influence of the frequency of the potential routine in the development of the Rh-II electrode evaluated through the parameter F; $A = 0.017$ cm^2

Discussion

Some considerations about the characterization of Rh surfaces

As far as we know, detailed surface studies of Rh single crystals of high-index Miller planes have not been reported. This fact contrasts with Pt, for which modern methods for surface research, including STM, have been applied, allowing the accurate identification of crystalline surface domains [4, 22, 23]. Nevertheless, STM has been employed only to investigate Rh(111) planes [35, 36, 37, 38]. Besides, the preparation of Rh single crystals faced some obstacles, because the cooling atmospheres used after the application of the flame annealing procedure [35, 39] are limited to $H_2 + Ar$ [35, 36, 37, 39] and $N_2 + Ar$ [38], taking into account that the surface is prone to oxidative restructuring [40].

Furthermore, the X-ray diffraction technique is of restricted application for the analysis of the electrofaceted metal surfaces since it informs about both the surface and the bulk of the metal. For this reason, in this work it was used only to characterize pc-Rh, because this electrode satisfies the condition required for the X-ray diffraction analysis concerning the distribution of crystalline planes. The results obtained for pc-Rh (Fig. 1e) exhibit peaks corresponding to (111), (200) and (220) planes in different intensity proportions than those expected for powder samples. The intensity of the (111) peak is very low and the one corresponding to (220) is the highest one, giving strong evidence for the prevalence of the (110) plane.

Table 2 Potentials for the H-electrosorption peaks of the different Rh surfaces studied

Surface	Peak potential (V)	
	H-electrodesorption	H-electroadsorption
pc-Rh	0.098[a], 0.134[a]	0.08, 0.11
Rh chemically etched	0.11	0.06
Rh-I	0.104	0.078
Rh-II	0.097	0.087
Rh-III	0.097[a], 0.104[a]	0.087[a], 0.078[a]

[a]Obtained by graphical deconvolution

On the other hand, for Rh-electrofaceted electrodes for which the depth of these surfaces involves a few monolayers and their structure is different to that of bulk metal, the application of X-ray diffraction analysis was ruled out. Therefore, the characterization of electrochemically modified Rh surfaces was mainly achieved employing cyclic voltammetry, Cu upd and SEM. In addition, graphical deconvolution of the voltammetric profiles has assisted in the identification of the different current contributions. The latter method has been successfully applied for Pt single crystals [41, 42, 43], and the fitting procedure using lorentzian curves has been shown to be satisfactory for the study of the H-electrosorption process on Pt [4].

Chemically etched Rh and electrofaceted Rh surfaces

The chemical etching of the pc-Rh surface in hot concentrated sulfuric acid led not only to a significant increase of the (111) planes, but also to the smoothing of the surface. The latter can be deduced from the width of the H-electrodesorption peak, which is distinctive for isoenergetic surface sites [44, 45].

In addition, the voltammetric features of electrofaceted Rh surfaces are rather different to those found for etched Rh surfaces. Thus, for the Rh-I electrode, which also exhibits a predominance of (111) planes, the H-electrodesorption peak is sharper than that of etched Rh surfaces, confirming the presence of stepped surfaces [17]. Furthermore, the peak potential is shifted towards more negative values, which indicates a decrease of the Rh-H_{ad} mean binding energy, and consequently an easier electrodesorption of H adatoms. This fact could be explained by considering that for this surface configuration the H atoms are adsorbed on steps and kinks, favouring a decrease of lateral interactions [46]. SEM micrographs have confirmed this stepped topography, where the surfaces are composed of a combination of high-index Miller Rh single crystals.

In accordance with the voltammetric behaviour of Rh(111) single crystals [30, 35], both (111) planes containing surfaces studied, i.e. Rh chemically etched and Rh-I surfaces, show a certain irreversibility in the H-electrosorption process. Moreover, as reported for Rh(110) single crystals [30], a higher reversibility for Rh-II electrodes is observed.

Previous results reported on Rh electrofaceting [24, 25] were devoted only to the H-electrosorption region, while the O-electrosorption region was disregarded. In the present work, particular attention was paid to the O-electrosorption potential domain because, in contrast to pc-Rh, the electrofaceted electrodes exhibit greater anodic charge densities related to O-containing species formed at $E > 0.8$ V, which are also responsible for the new cathodic current peaks IIc and IIIc. The O-con-

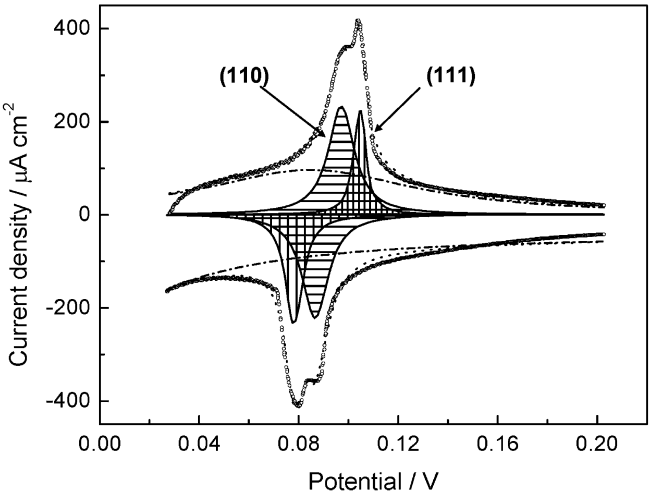

Fig. 5 Graphical deconvolution of the H-electrosorption region for Rh-III electrodes: *open circles*, experimental data; *dash dot*, contributions from hydrogen formation and oxidation; *horizonal pattern*, H-electrosorption peaks from (110) planes; *vertical pattern*, H-electrosorption peaks from (111) planes; *dashed line*, fitted curve to experimental data; $v = 0.1$ V s^{-1}, $A = 0.18$ cm^2

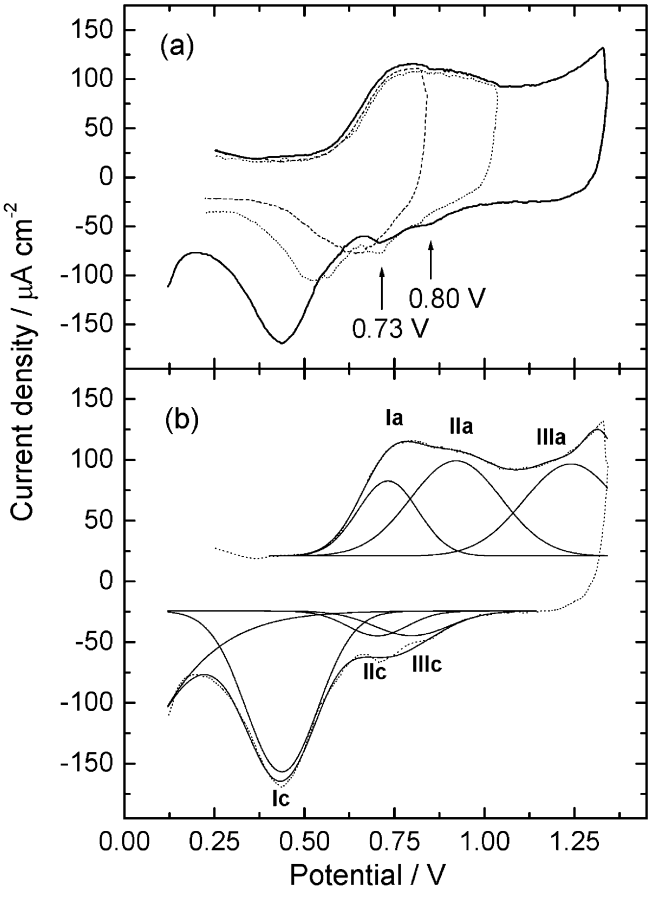

Fig. 6 **a** Cyclic voltammogram for O-electrosorption for Rh-I electrode obtained by a gradual change of the upper anodic switching potential, E_{sa}: *dashed line*, $E_{sa} = 0.8$ V; *dotted line*, $E_{sa} = 1.0$ V; *full line*, $E_{sa} = 1.3$ V. **b** Graphical deconvolution of the O-electrosorption region for $E_{sa} = 1.3$ V; I, II and III indicate current contributions; a = anodic, c = cathodic; $v = 0.1$ V s^{-1}, $A = 0.017$ cm^2

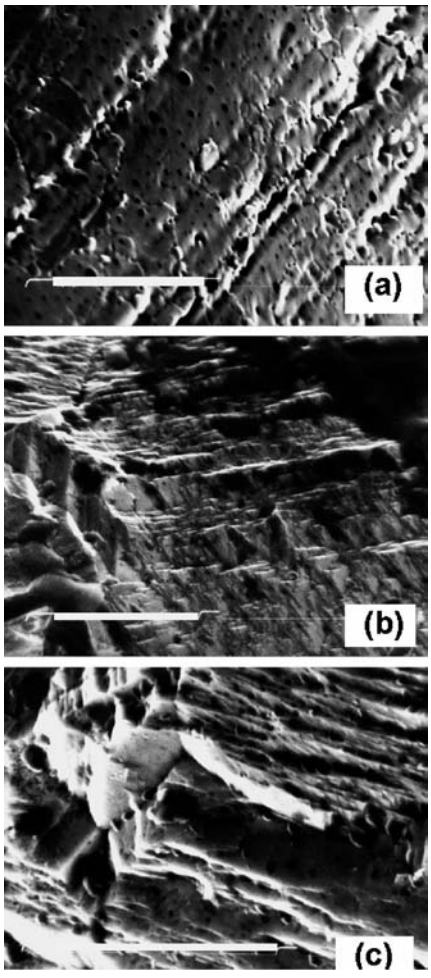

Fig. 7 SEM micrographs for (**a**) a pc-Rh electrode, (**b**) a Rh-I electrofaceted electrode and (**c**) a Rh-II electrofaceted electrode. *Bars* represent 10 μm

taining electrosorbed species would be formed at the surface defects, protecting these sites against the surface diffusion of Rh atoms and hence conferring higher stability to the electrofaceted surfaces. Thus, it is well known from surface diffusion studies, especially those concerning the mobility of surface atoms, either in vacuo or at metal|aqueous solution interfaces, that surface diffusion coefficients of metals, D_s, are affected by the applied potential, the electrolyte composition and the adsorbed species, producing a decrease of D_s [47, 48, 49].

Therefore, the solid surface cannot be taken as immutable anymore, but on the contrary, the so-called adsorbate-induced surface restructuring takes place [50]. The surface reconstruction is a function of the strength of the adsorbate-substrate interactions, as well as of the extent of the surface coverage with the interacting substances.

It should be noticed that there exists an adsorption-induced restructuring of the solid surfaces taking part in heterogeneous reactions, which is a consequence of the outward relaxation of surface atoms interacting with species in the gas phase or in an electrolyte [51]. Such a process implies a decrease in the strength of the interactions between surface and bulk atoms in the solid, with the consequence of an enhanced surface mobility of the corresponding species.

Mechanism of the electrofaceting process

According to the mechanism already proposed for the development of electrofaceted surfaces [52], the first step is related to the oxidation of Rh atoms. The standard potential for the different ionic species that could be formed are 0.7, 0.6 and 0.6 V for the redox couples Rh/Rh^{3+}, Rh/Rh^{2+} and Rh/Rh^{+}, respectively [53]. Although these data are given under thermodynamic conditions, it can be used as a first approximation to postulate that the formation of Rh^{+}, Rh^{2+} and Rh^{3+} could be favoured, although the Rh^{2+} species is unstable in aqueous solutions.

Within the anodic half-cycle the first stage expected to occur implies the interaction between Rh and the aqueous electrolyte:

$$Rh + H_2O \longrightarrow Rh(OH)_{ad} + H^+ + e^- \quad (1)$$

where OH species rearrange [54] at the surface while a fraction of the Rh atoms enter into the solution, undergoing metal electrodissolution according to:

$$Rh(OH)_{ad} \longrightarrow Rh^{3+} + OH^- + 2e^- \quad (2)$$

A subsequent reaction is accomplished:

$$Rh(OH)_{ad} \longrightarrow Rh(OH)_3 + 2H^+ + 2e^- \quad (3)$$

Moreover, at E_u the following reaction can take place:

$$2Rh(OH)_3 + Rh \longrightarrow 3RhO(OH) + 3H^+ + 3e^- \quad (4)$$

The formation of O-containing surface chemical species, $Rh(OH)_3$ and RhO(OH), was established through XPS and electrochemical studies [55, 56].

Otherwise, during the cathodic half-cycle, electrocrystallization of Rh^{3+} ions produced in the anodic half-cycle takes place:

$$Rh^{3+} + 3e^- \longrightarrow Rh^* \quad (5)$$

and also the electroreduction of the O-containing species:

$$3RhO(OH) + 3H^+ + 3e^- \longrightarrow 2Rh(OH)_3 + Rh^* \quad (6)$$

$$Rh(OH)_3 + 3H^+ + 3e^- \longrightarrow Rh^* + 3H_2O \quad (7)$$

Then, the overall process involved in one cycle can be described as electrooxidation/electroreduction reactions at the metal surface promoted by the periodic perturbing potential, resulting in a modified surface depicted as Rh*-containing atoms.

The occurrence of reactions (1) and (2) implies, in addition to the surface processes, the participation of mass transport in solution [57, 58]. In the absence of diffusing species in solution, the application of the potential routines for values of E_u and E_l lying above and below E_r, the equilibrium potential value for the Rh/Rh^{3+} redox couple, means that during the anodic half-cycle the electrode surface becomes a source of Rh^{3+} ions going into the solution. The maximum concentration gradient is then established between the electrode surface and the bulk of the solution through a distance δ_a, i.e. the corresponding boundary layer thickness. On the other hand, Rh^{3+} ion concentration at the electrode surface falls rapidly to zero during the cathodic half-cycle, provided the response of the Rh/Rh^{3+} redox couple is very fast. In this case, the concentration gradient of Rh^{3+} ions is established through the diffusional boundary layer thickness δ_c, which is much smaller than δ_a [57, 58].

Moreover, according to thermodynamic data the hydrogen evolution reaction should take place during the cathodic half-cycle. However, the occurrence of fast processes, as those related to the Rh/Rh^{3+} redox couple, are favoured by the high frequency employed, as it implies a short time spent at E_l. Furthermore, the influence of E_l can be better rationalized in terms of the factor W which is associated with the local electric field at the interface through the potential difference $[E_u–E_l]$, determining the electric driven force acting on the ions produced during the electrodissolution step. Taking into account the values of f and W, the ions produced during the anodic half-cycle remain at the interface, whereas, later on, owing to the high local electric field, they are driven to the surface during the cathodic half-cycle. Thus, the local electric field determines the speed at which these ions return to the surface, crystallizing either on low-energy (111) or on high-energy (110) surface sites (Table 1).

On the other hand, the voltammetric behavior of the electrofaceted metal can be explained by taking into account the restructured Rh* surface. Hence, the following oxidation sequence can take place during the positive-going potential scan up to $E = 1.2$ V:

$$Rh^* + H_2O \longrightarrow Rh^*(OH) + H^+ + e^- \quad (8)$$

$$Rh^*(OH) + 2H_2O \longrightarrow Rh^*(OH)_3 + 2H^+ + 2e^- \quad (9)$$

Reversing the potential scan, $Rh^*(OH)_3$ is electroreduced:

$$Rh^*(OH)_3 + 3H^+ + 3e^- \longrightarrow Rh^* + 3H_2O \quad (10)$$

In the negative-going potential scan there should be also considered the new cathodic current peaks IIc and IIIc, observed on faceted Rh-I and Rh-III and related to the O-electrodesorption process. Previous studies concerning the interaction of oxygen with Rh single crystals have shown that, on high-index Miller surfaces of Rh involving (111) planes on terraces, reconstruction leading to a reversible formation of double steps takes place [40]. Although this reconstruction has been observed for O-adsorption on the metal|gas interphase, it can be achieved when potential routines are applied to Rh|electrolyte interfaces. Thus, the double step formation is accomplished when a small amount of oxygen is adsorbed on the surface, about 0.1 ML, which is also expected to occur for the restructuring provoked by the fast periodic potential routine. Besides, the excess of O-atom adsorption takes place within the potential domain where peaks IIc and IIIc are observed and for which a charge of about 0.34 ML is involved, suggesting also the restructuring of pc-Rh.

Conclusions

The polycrystalline rhodium surface presents two energetically favourable sites for hydrogen electrosorption, exhibiting (110) and (100) symmetries. The topography of polycrystalline rhodium is modified by chemical etching with boiling concentrated sulfuric acid, yielding a smooth surface with predominance of (111) planes. The main consequence of this procedure is the redistribution of the original (110) sites, resulting from the surface diffusion of rhodium atoms to lower isoenergetic sites.

The application to polycrystalline rhodium electrodes of square wave potential routines, with the upper and lower potential limits located out of the thermodynamic stability of water, yields electrofaceted surfaces with a preferential surface orientation similar to those of high-index Miller planes containing mainly (110) and (111) basal crystallographic planes. The process of electrofaceting involves a sequence of electrooxidation/electroreduction reactions at the metal surface, resulting in three rhodium-modified surfaces. The potential difference $W = E_u–E_l$ induces a local electric field responsible for the reactions that take place in the anodic hemicycle, resulting in metal ions that enter into the solution and subsequently, in the cathodic hemicycle, return to the surface, crystallizing either on (111) or (110) surface sites.

Acknowledgements Financial support was provided by Fondo Clemente Estable no. 3037, PEDECIBA Programme (Uruguay), Consejo Nacional de Investigaciones Científicas y Técnicas (CONICET), Comisión de Investigaciones Científicas de la Provincia de Buenos Aires (CIC), and Facultad de Ciencias Exactas, Universidad Nacional de La Plata (Argentina). E.M., A.W.M. and C.F.Z. are members of the research career at PEDECIBA. A.M.C.L. is member of the research career at CIC. M.E.M. is member of the research career at CONICET.

References

1. Leiva EPM, Santos E, Cerviño RM, Giordano MC, Arvia AJ (1985) Electrochim Acta 30:1111
2. Arévalo MC, Gomis-Bas C, Hahn F, Beden B, Arévalo A, Arvia AJ (1994) Electrochim Acta 39:793

3. Zinola CF, Castro Luna AM, Triaca WE, Arvia AJ (1994) Electrochim Acta 39:1627
4. Martins ME, Zinola CF, Andreassen G, Salvarezza RC, Arvia AJ (1998) J Electroanal Chem 445:135
5. Méndez E, Martins ME, Zinola CF (1999) J Electroanal Chem 477:41
6. Zubimendi JL, Andreassen G, Triaca WE (1995) Electrochim Acta 40:1305
7. Cerviño RM, Triaca WE, Arvia AJ (1985) J Electrochem Soc 132:266
8. Vázquez L, Gómez J, Baró AM, García N, Marcos ML, González Velasco J, Vara JM, Arvia AJ, Presa J, García A, Aguilar M (1987) J Am Chem Soc 109:1730
9. Bittins-Cattaneo B, Santos E, Vielstich W (1986) Electrochim Acta 31:1495
10. Albano EV, Martin HO, Arvia AJ (1988) Electrochim Acta 33:271
11. Custidiano E, Kessler T, Triaca WE, Arvia AJ (1986) Electrochim Acta 31:1671
12. Egli WA, Visintin A, Triaca WE, Arvia AJ (1993) Appl Surf Sci 68:583
13. El-Shafei AA, Ohmori T, Enyo M (1994) J Electroanal Chem 379:247
14. Gómez J, Vazquez L, Baró AM, Perdriel CL, Arvia AJ (1989) Electrochim Acta 34:619
15. Perdriel CL, Ipohorski M, Arvia AJ (1986) J Electroanal Chem 215:317
16. Arvia AJ, Canullo JC, Custidiano E, Perdriel CL, Triaca WE (1986) Electrochim Acta 31:1359
17. Canullo JC (1993) PhD Thesis, Universidad Nacional de La Plata, Argentina
18. Castro Luna AM, Zinola CF (1997) J Braz Chem Soc 8:102
19. Gómez J, Vazquez L, Baró AM, García N, Perdriel CL, Triaca WE, Arvia AJ (1986) Nature 323:612
20. Motoo S, Furuya N (1987) Ber Bunsenges Phys Chem 91:457
21. Méndez E (2001) PhD Thesis, Universidad de la República, Uruguay
22. Furuya N, Ichinose M, Shibata M (1999) J Electroanal Chem 460:251
23. Furuya N, Shibata M (1999) J Electroanal Chem 467:85
24. Canullo JC, Custidiano E, Salvarezza RC, Arvia AJ (1987) Electrochim Acta 32:1649
25. Custidiano E, Piovano S, Arvia AJ, Chialvo AC, Ipohorski M (1987) J Electroanal Chem 221:229
26. Rand DAJ, Woods R (1971) J Electroanal Chem 31:29
27. Pallota C, de Tacconi NR, Arvia AJ (1981) Electrochim Acta 26:261
28. Pallota C, de Tacconi NR, Arvia AJ (1983) J Electroanal Chem 159:201
29. Jerkiewicz G (1996) J Phys Chem 100:8454
30. Lapa AS, Safonov VA, Petrii OA, Korenovskii NL (1984) Elektrokhimiya 20:1550
31. Zelenay P, Horányi G, Rhee CK, Wieckowski A (1991) J Electroanal Chem 300:499
32. Krauskopf EK, Wieckowski A (1992) In: Lipkowski J, Ross PN (eds) Adsorption of molecules at metal electrodes. VCH, Weinheim
33. Horányi G, Wasberg M (1996) J Electroanal Chem 404:291
34. Wasberg M, Hourani M, Wieckowski A (1990) J Electroanal Chem 278:425
35. Clavilier J, Wasberg M, Petit M, Klein LH (1994) J Electroanal Chem 374:123
36. Wan LJ, Yau SL, Itaya K (1995) J Phys Chem 99:9507
37. Wan LJ, Yau SL, Swain GM, Itaya K (1995) J Electroanal Chem 381:105
38. Itaya K (1998) Prog Surf Sci 58:121
39. Clavilier J (1980) J Electroanal Chem 107:211
40. Cornelli G, Dhanak VR, Kiskinova M, Prince KC, Rosei R (1998) Surf Sci Rep 32:165
41. Armand D, Clavilier J (1987) J Electroanal Chem 225:205
42. Armand D, Clavilier J (1987) J Electroanal Chem 233:251
43. Loeve B, Seto K, Lipkowski J (1986) J Electroanal Chem 199:219
44. Vanselow R, Li XOD (1992) Surf Sci Lett 264:L200
45. Bernasck SL, Siekhaus WJ, Somorjai GA (1973) Phys Rev Lett 30:1202
46. Koeleman BJJ, Zwart ST, Boers AL, Poelsema B, Verhey LK (1983) Nucl Instrum Methods Phys Res 218
47. Salvarezza RC, Arvia AJ, Vara JM (1992) Electrochim Acta 37:2205
48. García MP, Gómez MM, Salvarezza RC, Arvia AJ (1993) J Electroanal Chem 347:237
49. Doña JM, González Velasco J (1992) Surf Sci 274:205
50. Somorjai GA, Van Hove MA (1989) Prog Surf Sci 30:201
51. Somorjai GA (1990) J Phys Chem 94:1013
52. Arvia AJ, Salvarezza RC, Triaca WE (1989) Electrochim Acta 34:1057
53. Milazzo G, Caroli S (1978) Tables of standard electrode potentials. Wiley, Chichester
54. Angerstein-Kozlowska H, Conway BE, Sharp WBA (1973) J Electroanal Chem 43:9
55. Peuckert M (1984) Surf Sci 141:500
56. Villiard F, Jerkiewicz G (1997) In: Jerkiewicz G, Soriaga MP, Uosaki K, Wieckowski A (eds) Solid-liquid electrochemical interfaces. (ACS symp ser 656) American Chemical Society, Washington, pp 323
57. Elsner CI, Perdriel CL, Marchiano SL, Arvia AJ (1990) Electrochim Acta 35:215
58. Marchiano SL, Rebollo Neira L, Arvia AJ (1990) Electrochim Acta 35:483